FERMILAB-PUB-11-551-CD

A Closer Look at the 2011 cMSSM Results from CMS

Stephen Mrenna

SSE Group,
Computing Division,
Fermilab,
Batavia, IL 60510

E-mail: mrenna@fnal.gov

Abstract: We present a phenomenological appraisal of the results of several searches for Supersymmetry (SUSY) performed at the LHC by the CMS collaboration and interpreted in the context of the cMSSM. Part of the analysis focuses on which SUSY production processes are being probed. We observe that much of the current exclusion region is dominated by squark-squark and squark-gluino production, and explain the shape of the exclusion curves. Based on this analysis and an estimation of future reach, additional simplified models are suggested. Other phenomenological details are discussed, such as the effect of radiation on acceptance.

Contents

1 Introduction

Significant effort at the LHC is dedicated to analyzing data to find evidence of, or to exclude, models of Supersymmetry (SUSY) (Refs. [1, 2] provide thorough theoretical reviews.) Many of the results of these analyses are interpreted in the context of the constrained Minimal Supersymmetric Standard Model (cMSSM) [3], with exclusion contours shown in the plane of the universal scalar mass m_0 and the gaugino mass $m_{\frac{1}{2}}$ parameters, with other cMSSM parameters fixed ($\tan\beta, A_0, sgn(\mu)$). A recent result from CMS [4] is presented in Fig. 1, based on 1.1 fb^{-1} of data.

Our initial attention is drawn to the curves in Fig. 1 labeled *Jets+mHT* [5], α_T [6], and *MT2* [7], referring to limits from specific analyses known by those colloquial names. These analyses are sensitive mainly to the production and hadronic decays of sparticles, whereas the other analyses, with limit contours labeled *1 Lepton*, *SS/OS Dilepton*[8–10], depend explicitly on branching fractions of sparticles to leptons (either directly or through decays of gauge bosons).

The hadronic limits demonstrate that:

- for low m_0, there is a significant reach in $m_{\frac{1}{2}}$ ($\sim$ 540 GeV);
- for large m_0, $m_{\frac{1}{2}}$ is limited to smaller values ($\sim$ 300 GeV).

The parameters m_0 and $m_{\frac{1}{2}}$ are *not* the physical masses of the theory, which set the size of production cross sections and the kinematics of decays. However, $M_{\widetilde{g}}$ is basically set by $m_{\frac{1}{2}}$ ($M_{\widetilde{g}} \sim 2.5 m_{\frac{1}{2}}$), while ${M_{\widetilde{q}}}^2$ has a quadratic dependence on m_0 and $m_{\frac{1}{2}}$. From Fig. 1, it is clear that the excluded gluino mass is not a flat line: the exclusion depends strongly on the squark mass. (Figure 18 of the Appendix shows the correlations between $M_{\widetilde{g}}$ and $M_{\widetilde{q}}$ in the $(m_0, m_{\frac{1}{2}})$ plane relevant for this analysis.) In particular, one can see from the contours of fixed gluino and squark mass, labeled $\widetilde{q}$ and $\widetilde{g}$, that $M_{\widetilde{q}} < 1$ TeV is excluded regardless of $M_{\widetilde{g}}$, whereas $M_{\widetilde{g}} < 1$ TeV is only excluded for $M_{\widetilde{q}} <$1.1 TeV. The exclusion curve seems to follow the semi-circular contours of fixed $M_{\widetilde{q}}$ for low $m_0 < 1$ TeV, and the flat contours of fixed $M_{\widetilde{g}}$ for larger m_0.

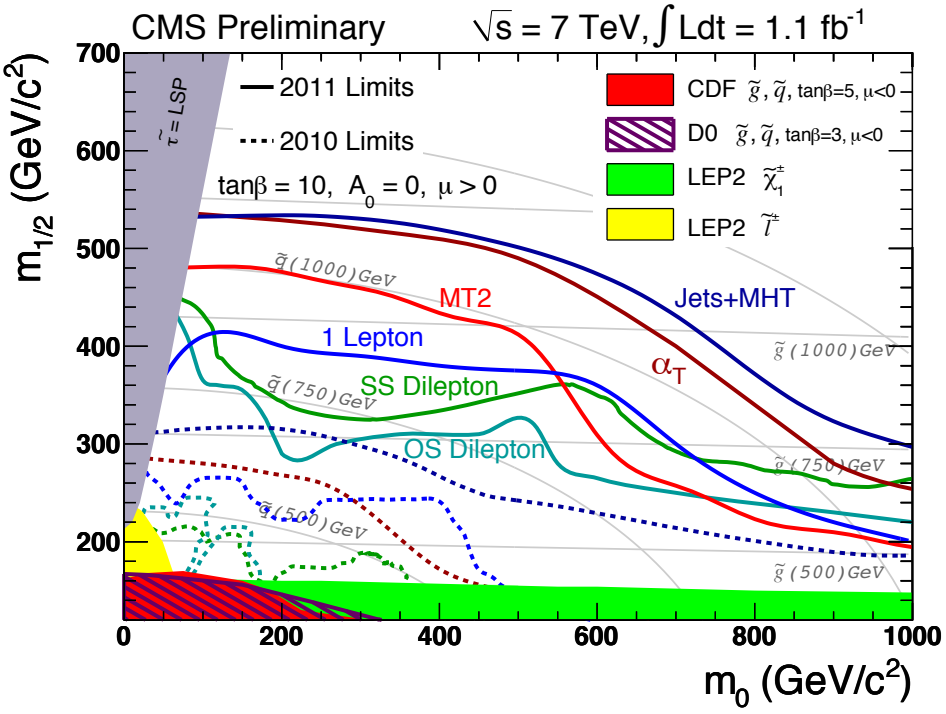

Figure 1. Observed limits from several 2011 CMS SUSY searches plotted in the cMSSM $(m_0, m_{\frac{1}{2}})$ plane, with $\tan\beta = 10, A_0 = 0, sgn(\mu) > 0$.

The physical masses of the cMSSM are highly correlated, as expected from a model that has many observables but only a few parameters. While the quantitative structures of the cMSSM depend on the exact specification of $m_0, m_{\frac{1}{2}}, A_0, \tan\beta, sgn(\mu)$, the qualitative features are set by m_0 and $m_{\frac{1}{2}}$ (for larger values of $\tan\beta$, third generation sparticles may be lighter. From the collider physics phenomenology point of view, this affects the other spectra mildly, but can have significant implications for decay modes.) It is well known that $M_{\tilde{q}} > M_{\tilde{g}}$ in most of this plane and that the gaugino masses come in specific ratios ($M_{\widetilde{N}_1} \equiv M_{\widetilde{\chi}_1^0} \sim \frac{1}{6} M_{\tilde{g}}$). One can question whether general results can be learned from examining the limits within the cMSSM, and for a single choice of cMSSM parameters. In particular, this limit is for $\tan\beta = 10, A_0 = 0$ GeV, $sgn(\mu) > 0$. (We also comment on the case of $\tan\beta = 40, A_0 = -500$ GeV, $sgn(\mu) > 0$.) We argue that several lessons can be learned from this particular cMSSM interpretation, despite the fact that it is explicitly model-dependent.

In this paper, we will investigate:

1. the dominant SUSY processes that contribute to these limits. In particular, we would like to understand the shape of the CMS exclusion curves in Fig. 1. Analyzing the plane this way is a mapping of a point in $(m_0, m_{\frac{1}{2}})$ into simple or simplified models;

2. the impact of this mapping on the selection of simplified models for future studies to better understand the experimental results;

3. the sensitivity of the various analyses to specific SUSY production processes and decay modes;

4. phenomenological details relevant to this analysis and other new particle searches, such as kinematic features of various processes and the role of radiation in searches.

2 Dominant Processes

The purpose of this section is to examine which processes are contributing to our current exclusion contours in the cMSSM. Here, we concentrate on the size of production cross sections without consideration of a specific selection of events, as in a search analysis. We will justify this later. The deconstruction of the cMSSM into subprocesses is a mapping into a set of simplified model spectra (SMS) (see [17], for example). This will help us to understand the generality of these cMSSM results, and interpret them in simplified models. The main result is presented in Fig. 2, which shows the fractional importance of various SUSY pair production processes as a function of $(m_0, m_{\frac{1}{2}})$ for the same parameters as in Fig. 1.

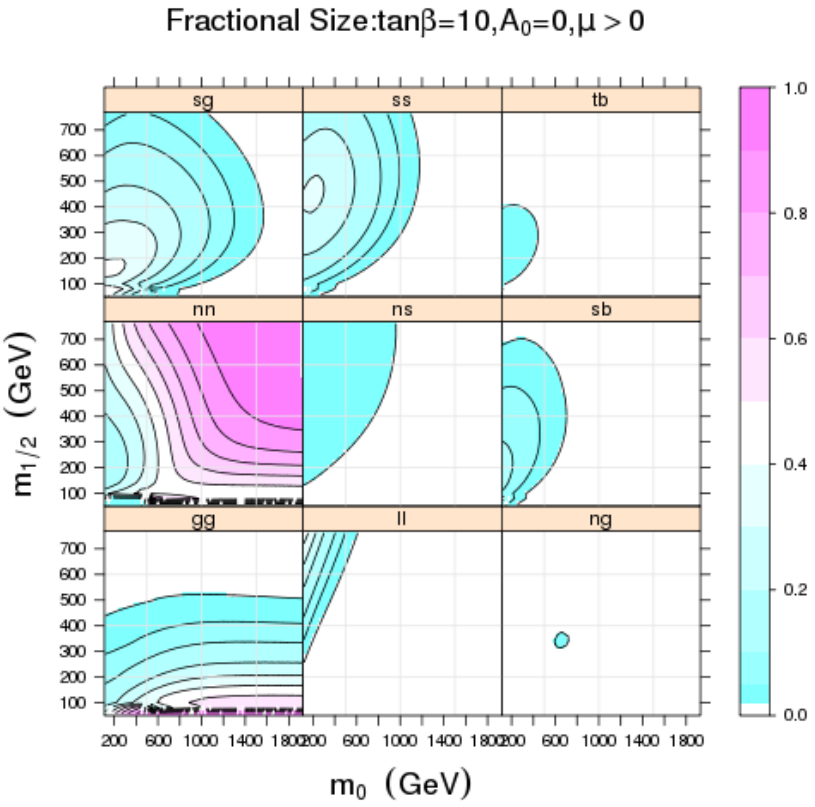

Figure 2. Fractional size of various subprocesses as a function of $(m_0, m_{\frac{1}{2}})$ for $\tan\beta = 10, A_0 = 0$ GeV, $sgn(\mu) > 0$.

The labels in Fig. 2 represent (from top-left to bottom-right) the following production processes: sg = squark-gluino, ss = squark-squark, tb = stop-antistop, nn = neutralino/chargino pair, ns = neutralino/chargino-squark, sb = squark-antisquark, gg = gluino pair, ll = slepton-antislepton, ng = neutralino/chargino-gluino. The classifications sum over similar processes: nn, for example, includes

all $\widetilde{N}_i\widetilde{N}_j, \widetilde{C}_i\widetilde{C}_j, \widetilde{N}_i\widetilde{C}_j$ processes. (In practice, only a few processes tend to saturate the sum, e.g. $\widetilde{C}_1\widetilde{N}_2$ and $\widetilde{C}_1\widetilde{C}_1$ in this case.) For brevity, the mostly-negligible sbottom-antisbottom pair production is not shown in Fig. 2. These and other production cross sections were calculated using the computer code `Prospino` to NLO accuracy [11]. The physical particle properties were calculated using the MSSM evolution code `SoftSUSY` [12], while sparticle and Higgs boson decays widths were calculated from `SUSYHIT` [13] (sparticle decays are considered later).

The all-hadronic searches naively target squark and gluino production. Figure 2 demonstrates that squark-squark production and squark-gluino production have large rates at small m_0. For small $m_{\frac{1}{2}}$, gluino pair production is important, while the production of electroweak gauginos is important, if not dominant, over most of the plane.

For further clarity, we focus on the largest process at each point in the plane, which is presented in Fig. 3. Only four classes of processes every satisfy the criterion of being the largest cross section

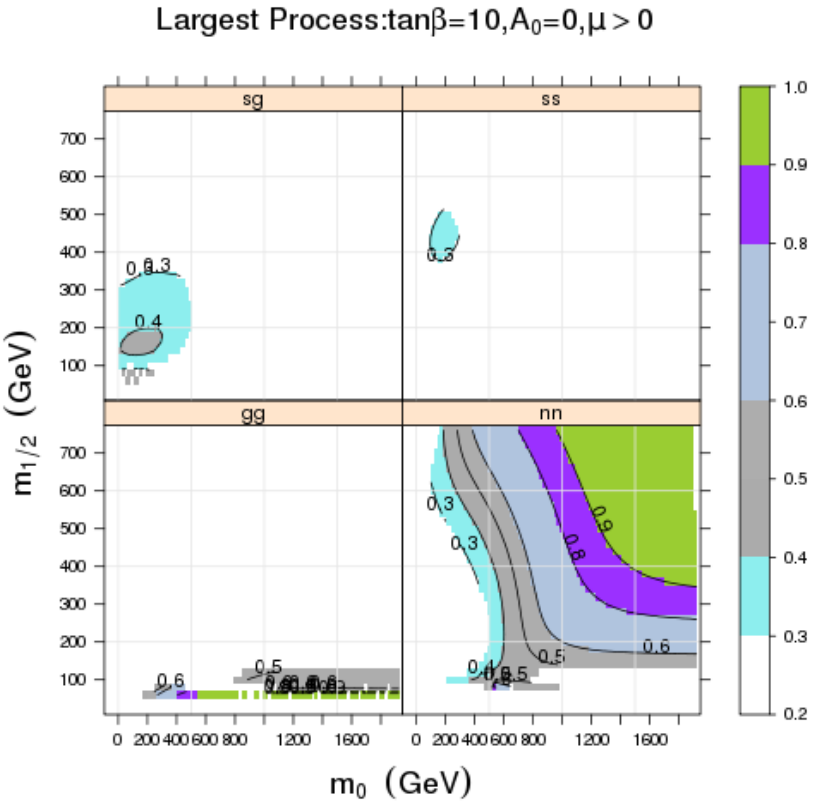

Figure 3. The largest cross section in the $(m_0, m_{\frac{1}{2}})$ plane, with contours showing the fractional size.

at any point (a small region of slepton production for small m_0 and large $m_{\frac{1}{2}}$ is not shown). When squark-squark production is the largest (roughly $400 < m_0 < 500$ GeV, $100 < m_{\frac{1}{2}} < 300$ GeV), it comprises 30-40% of the total Susy rate at that point.[1] Gluino-pair production is largest in only

[1]The large contribution of *ss* processes to the total SUSY production cross section was noted for the LM1 benchmark point in Ref. [20].

a limited region of $m_{\frac{1}{2}}$ (roughly $m_{\frac{1}{2}} < 120$ GeV); the other gauginos have much more significant production rates. Clearly, searches that are sensitive to the electroweak gaugino processes (mainly $\widetilde{C}_1^{\pm}\widetilde{C}_1^{\mp}, \widetilde{C}_1^{\pm}\widetilde{N}_2$) can gain inroads to the upper-right portion of the plane. sg is competitive with ss, and the largest process for a the region $m_0 < 400$ GeV, $100 < m_{\frac{1}{2}} < 300$ GeV. We reproduce Fig. 2 for the case of large $\tan\beta$, namely $\tan\beta = 40, A_0 = -500$ GeV, $sgn(\mu) > 0$, in Fig. 20 of the Appendix. The qualitative behavior is the same.

These conclusions are noteworthy. First, squark-squark production can only occur if a gluino exists, whereas squark-antisquark production arises directly from the QCD Lagrangian. Even if the gluino is heavy enough to have a suppressed production cross section, the squark-squark production cross section can be substantial (we study this more quantitatively later). Thus, an indirect way to prove or disprove the existence of a gluino with a TeV-scale mass is to establish that a signal is squark-squark or squark-antisquark production. Potential clues could be obtained through jet-charge or exploiting some differences in gluon radiation arising from the contributions of valence or sea quarks to the process (see later discussion).

Squark-gluino production, squark-squark, and gluino-gluino production processes are all competing at once. We will investigate what mass relations between the squark and gluino allow squark-gluino production to dominate over the other possible production processes.

The nn processes are mainly the SUSY duals of WW and WZ production, which is typical of the cMSSM. Almost all of nn is $\widetilde{C}_1^{\pm}\widetilde{N}_2$ and $\widetilde{C}_1^{\pm}\widetilde{C}_1^{\mp}$ production, with the lightest chargino $\widetilde{C}_1$ and the second heaviest neutralino $\widetilde{N}_2$ nearly degenerate in mass.

The cross sections for stop and sbottom pair production are never competitive with other processes (even with $\tan\beta = 40$) for these cMSSM parameters. We will discuss this more later.

The *total* SUSY production cross section in the $(m_0, m_{\frac{1}{2}})$ plane is presented in Fig. 4. The contours of constant cross section are nearly horizontal lines in $m_{\frac{1}{2}}$. This is not surprising, since the cross section for the nn process is set mainly by the chargino and neutralino masses. Comparing with the limits in Fig. 1 (and reproduced in this figure), we observe that current searches with 1.1 fb^{-1} of data are excluding the cMSSM points that yield a total cross section of several hundred fb, or several hundred SUSY events before event selection.

3 Simplified Models

The simplified model approach originated as a topological classification of signals to allow hypothesis testing [15, 16]. It is based on the observation that the kinematics of new particle production and decay is often characterized by the mass scales involved, and not by the particulars of matrix elements. In the absence of signals, simplified models (SMS) can be used to present results with less model dependence [17]. Thus, SUSY search limits can be recycled to provide information to the community about the dependence of these limits on the masses and decay chains in a particular model. SMS are also useful to the analysts, since it reveals the coverage of the cuts used in a particular analysis.

By breaking down the results in the cMSSM into individual processes, we are mapping into simplified models. Do we have the right ones or enough?

This simple analysis of only the production cross sections can already have an impact on the choice of simplified models used to interpret the data. The main suggested topologies, $\widetilde{g}\widetilde{g}$ and $\widetilde{q}\widetilde{q}^*$ [19], are not the most relevant in most of the cMSSM plane, even though we have relied on these processes to motivate our initial choices of topologies. If our aim is to provide motivated SMS that cover the main possibilities in a model like the cMSSM, and/or to allow for the deconstruction of a particular point in the cMSSM plane in terms of SMS, then other topologies need to be considered, such as:

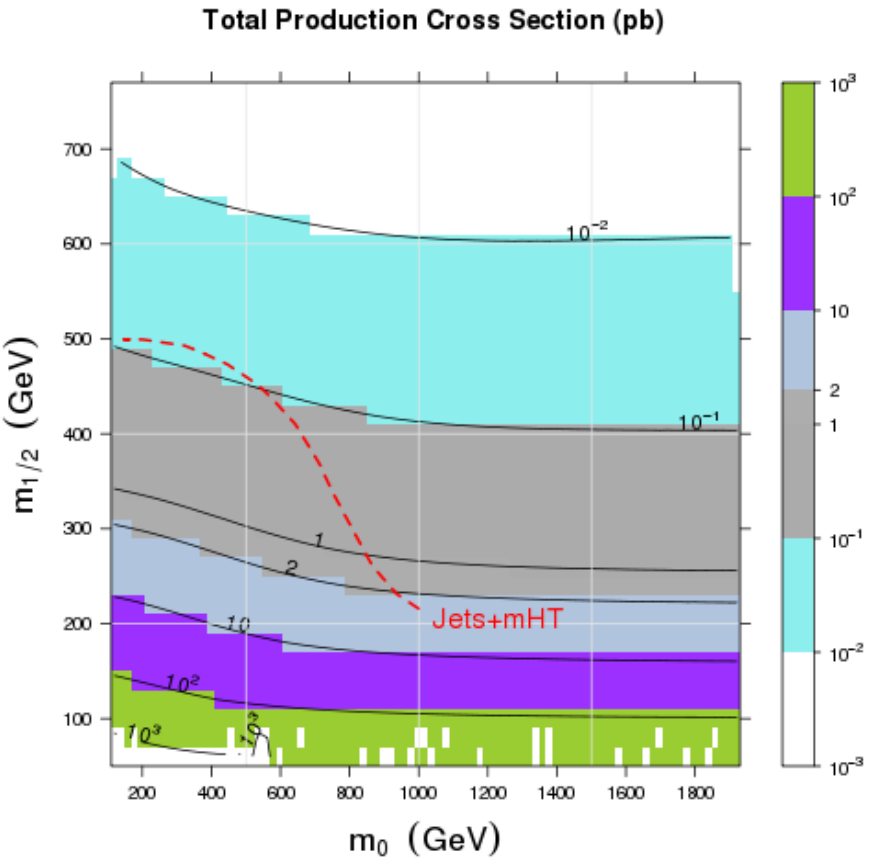

Figure 4. The total SUSY production cross section as a function of $(m_0, m_{\frac{1}{2}})$ in the cMSSM for $\tan\beta = 10, A_0 = 0$ GeV, $sgn(\mu) > 0$. The strongest limit curve from Fig. 1 is overlaid with the label *Jets+mHT*.

1. squark-squark (ss) production;
2. squark-gluino (sg) production;
3. Weak gaugino (nn) production, like $\widetilde{C}_1^{\pm}\widetilde{C}_1^{\mp}$ and $\widetilde{C}_1^{\pm}\widetilde{N}_2$.

However, there are caveats. A specific point in the $(m_0, m_{\frac{1}{2}})$ plane will likely not have the simple structure of the simplest of SMS, with a single decay chain. Instead, cascade decays like $\widetilde{q}_R \to q\widetilde{N}_2, \widetilde{q}_L \to q\widetilde{N}_2, q\widetilde{C}_1$ are competing with single step decays like $\widetilde{q} \to q\widetilde{N}_1$. In general, cascade decays tend to soften the $\not{E}_T$ spectrum, but can provide more jets that increase acceptance. Thus, limits in the SMS may be different than those in the cMSSM for similar choices of $M_{\widetilde{q}}, M_{\widetilde{g}}, M_{\widetilde{N}_1}$.

First, we examine the $\widetilde{q}\widetilde{q}$ process and compare the kinematics of $\widetilde{q}\widetilde{q}$ and $\widetilde{q}\widetilde{q}^*$ production. We expect some differences from the effect of the parton distribution functions, since valence-valence quark scatterings can only contribute to $\widetilde{q}\widetilde{q}$ production. Differences arise at the hard-process level, but also from initial state radiation.

Figure 3 shows comparisons of the $\widetilde{q}$ (or $\widetilde{q}^*$) p_T after the hard event and parton shower generation from `Pythia` (see the Appendix for details). Comparisons of the rapidity are also shown in the

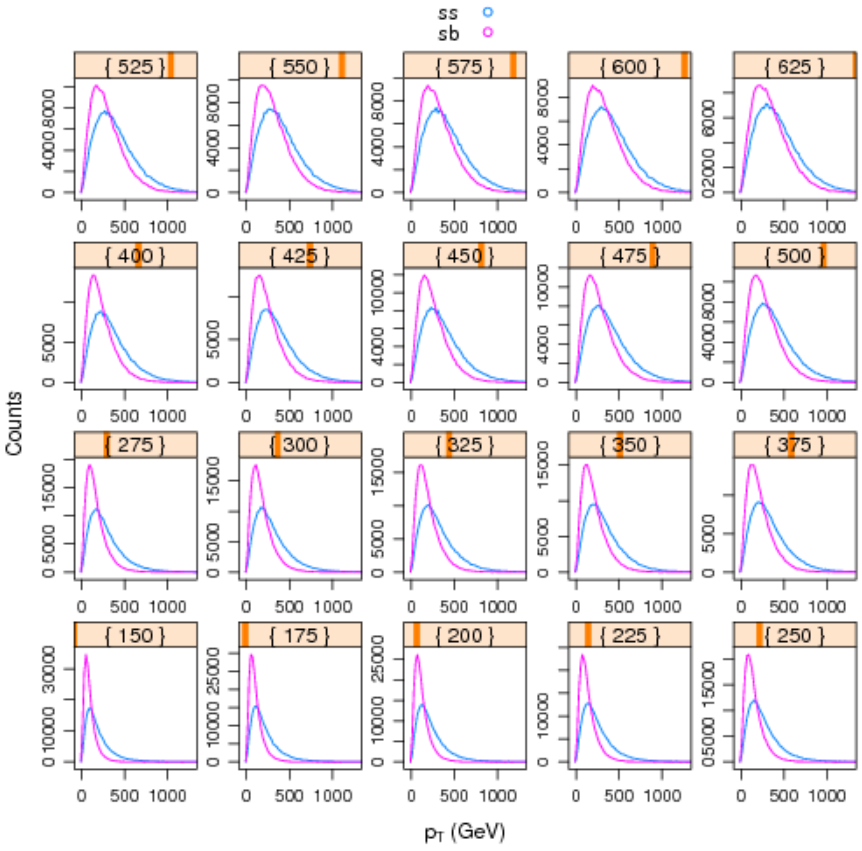

Figure 5. Comparison of the transverse momentum p_T of the produced $\widetilde{q}, \widetilde{q}^*$. Plots of rapidity y are shown in the Appendix.

Appendix. Values of $150 \leq M_{\widetilde{q}} \leq 650$ GeV are displayed, though we have studied larger values. In general, differences are less pronounced for larger $M_{\widetilde{q}}$. For $M_{\widetilde{q}} < 800$ GeV, the p_T of the squark is harder for *ss* production, while the rapidity y is less central. Thus, the acceptance of *ss* events should be different from *sb*. If the acceptance is also dependent upon a jet arising from initial state radiation, there will be further differences.

Since interpretations of data with simplified models have been presented only for $\widetilde{g}\widetilde{g}$ and $\widetilde{q}\widetilde{q}^*$ topologies so far (see, for example, Ref. [21]), we encourage a study of $\widetilde{q}\widetilde{q}$ topologies. However, as a first estimate, one can ignore the differences in acceptance, and interpret the data using *ss* cross sections, instead of *sb*. This requires a choice of $M_{\widetilde{g}}$, since the *ss* cross section vanishes otherwise. We have checked that the kinematic dependence on $M_{\widetilde{g}}$ is negligible, and the $\widetilde{q}\widetilde{q}$ acceptance for $M_{\widetilde{g}} = 2$ TeV is nearly identical to that for $M_{\widetilde{g}} = 4$ TeV, so that signal events can be studied "independently" of $M_{\widetilde{g}}$. Later, we will see that the *ss* cross section exceeds the *sb* one even for cases when $M_{\widetilde{g}}$ is quite large.

Next, we turn to the squark-gluino process. We consider the complete MSSM description of squarks and gluinos, so that all production cross sections are competing and interconnected. We have

discussed already the $\widetilde{g}\widetilde{g}$, $\widetilde{q}\widetilde{q}$, and $\widetilde{q}\widetilde{q}^*$ contributions. In Figure 6, we show the relative size of each cross section as a function of the mass splitting between the gluino and squark, for several fixed values of $M_{\widetilde{q}}$. *sg* is the dominant production process in a small window, roughly near $M_{\widetilde{g}} \sim M_{\widetilde{q}}$, that changes moderately with $M_{\widetilde{q}}$. For low $M_{\widetilde{q}}$, the dominance occurs for nearly degenerate squarks and gluinos.

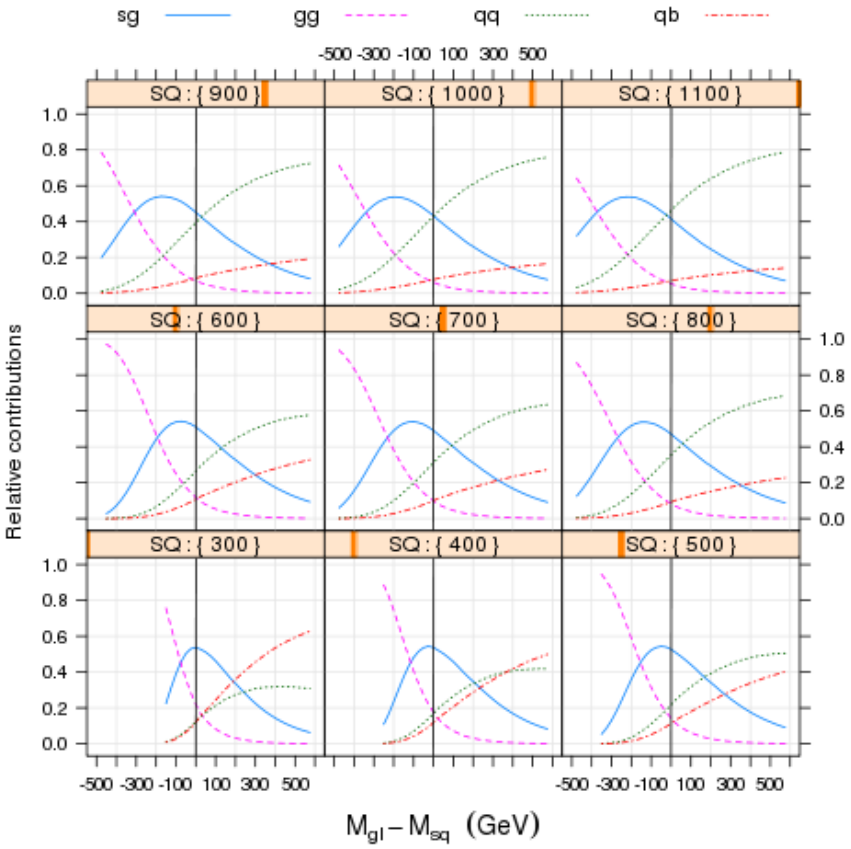

Figure 6. The relative SUSY QCD production cross sections as a function of the mass splitting between the gluino and squark. The vertical line is for degenerate $M_{\widetilde{q}}, M_{\widetilde{g}}$.

However, for higher $M_{\widetilde{q}}$, the maximum occurs when the gluino is somewhat lighter than the squarks. This leads to a parton-level signature of $\widetilde{q}(\to q\widetilde{g}(\to q\bar{q}\widetilde{N}_1)\widetilde{g}(\to q\bar{q}\widetilde{N}_1)$. Of course, specific cuts might select *sg* over other topologies, so it could be important even what it is not the largest cross section. This suggests SMS with $M_{\widetilde{g}}$ within ± 200 GeV of $M_{\widetilde{q}}$. We note also the rise of $\widetilde{q}\widetilde{q}$ over $\widetilde{q}\widetilde{q}^*$ production once $M_{\widetilde{q}} > 500 - 600$ GeV. For $M_{\widetilde{q}} = 600$ GeV and $M_{\widetilde{g}} = 1200$ GeV, the $\widetilde{q}\widetilde{q}$ production cross section is roughly 0.5 pb.

In Figure 7, we present the same information as a contour plot in the $M_{\widetilde{q}}, M_{\widetilde{g}}$ plane. Note the unequal limits for each axes, chosen to emphasize the size of the $\widetilde{q}\widetilde{q}$ cross section for large $M_{\widetilde{g}}$. Focusing on the behavior of the $\widetilde{q}\widetilde{q}$ cross section at fixed $M_{\widetilde{q}} = 400$ GeV as a function of $M_{\widetilde{g}}$, one observes a decrease of only one order of magnitude in the cross section as the $M_{\widetilde{g}}$ varies from 275 to 2000 GeV.

Next, we comment on electroweak gaugino pair production. In the cMSSM, the mass splitting

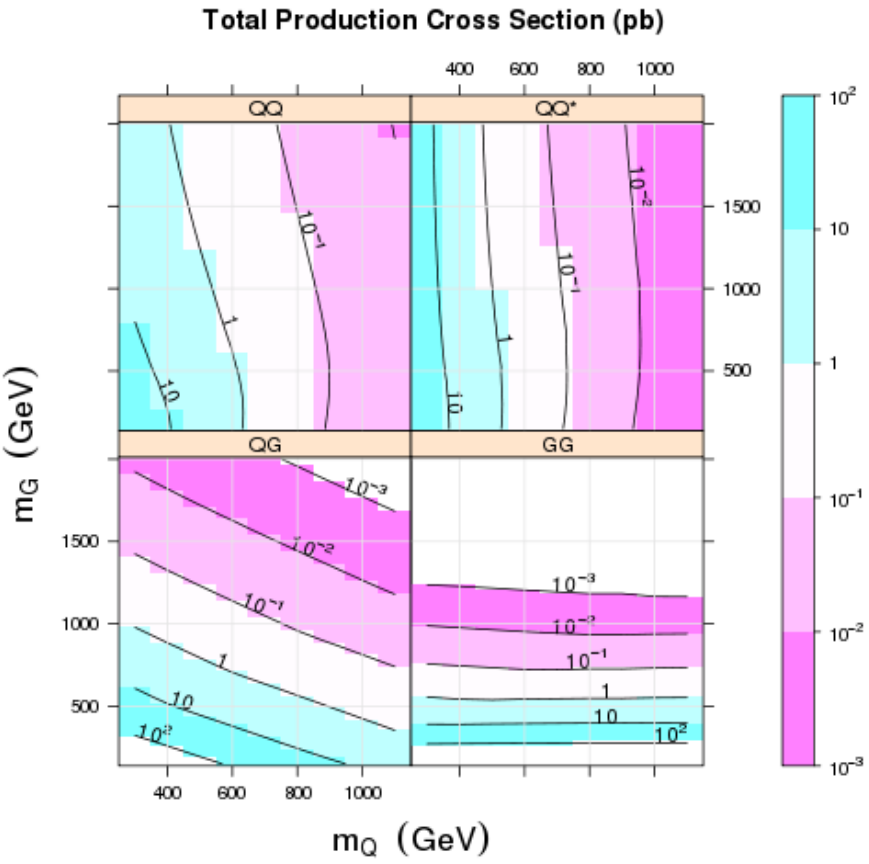

Figure 7. Levels of SUSY QCD production cross sections as a function of the gluino and squark masses.

between the chargino ($\sim 0.8 m_{\frac{1}{2}}$) and the LSP ($\sim 0.4 m_{\frac{1}{2}}$) is roughly $0.4 m_{\frac{1}{2}}$. Once $m_{\frac{1}{2}} > M_W/0.4 \sim 200$ GeV, the decay $\widetilde{C}_1 \to W\widetilde{N}_1$ is allowed for on-shell particles. From Fig. 1, we observe that the current leptonic analyses are *already* limiting models of this type, since their contours extend up to and beyond $m_{\frac{1}{2}} \sim 200$ GeV. (We have not studied in detail the shapes of the leptonic limits, but leave this for a future study.) This may be viewed as a worst-case in terms of leptonic branching ratio (at specific points, $\widetilde{N}_2 \to \widetilde{N}_1 h(\to b\bar{b})$ can occur. We comment on this later). Even hadronic searches may be sensitive to these processes, which naively yield 4 hard jets and $\not{E}_T$. For heavy enough $\widetilde{C}_1$ and $\widetilde{N}_2$, the gauge bosons produced in decays may be significantly boosted.

In Figure 8, we show contours of significant decays modes of $\widetilde{C}_1$ and $\widetilde{N}_2$ for $\tan\beta = 10, A_0 = 0, sgn(\mu) > 0$. The contour of $BR(\widetilde{C}_1 \to W\widetilde{N}_1) \sim 1$ is the solid, black line near $m_{\frac{1}{2}} \sim 200$GeV – our naive expectation of where this decay should turn on. The region where $\widetilde{N}_2 \to Z\widetilde{N}_1$ is significant is small and enclosed by the blue, long–dashed line, and its lower bound is near the start of the $\widetilde{C}_1$ contour. Near $m_{\frac{1}{2}} \sim 300$GeV, a new decay mode is dominant, namely $\widetilde{N}_2 \to h\widetilde{N}_1$. This has a (negative) impact on multi-lepton searches, but also opens the possibility of a $Wh\not{E}_T$ signal. The dominance of $\widetilde{N}_2 \to h\widetilde{N}_1$ is a feature, or peculiarity, of the correlations inherit to a model like the cMSSM, with only a few input parameters. A reasonable extension of the cMSSM is to decouple the

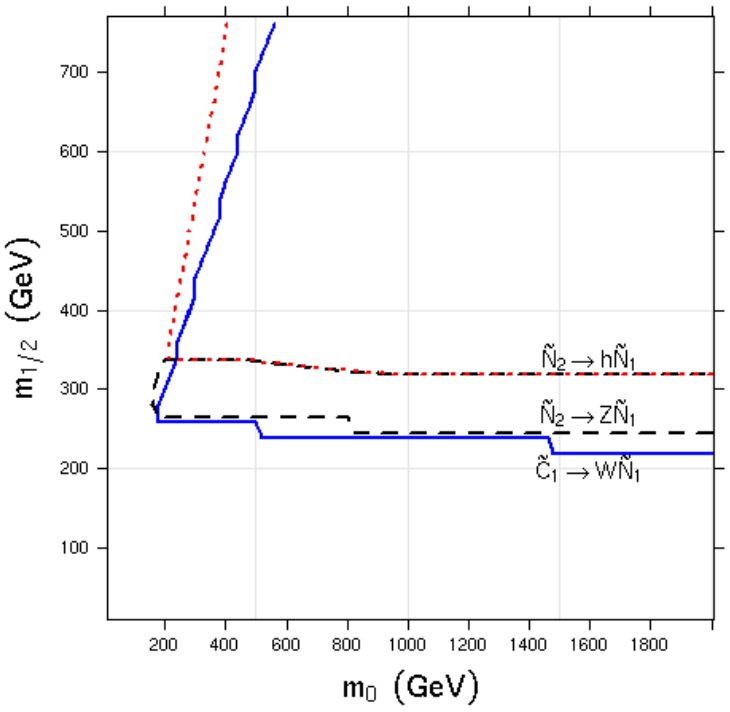

Figure 8. Regions where BR($C_1 \to WN_1$), BR($N_2 \to ZN_1$), and BR($N_2 \to hN_1$) are significant in the $(m_0, m_{\frac{1}{2}})$ plane for $\tan\beta = 10, A_0 = 0$ GeV, $sgn(\mu) > 0$.

Higgs scalar from the sfermion scalar parameter. A simple treatment, suitable for collider physics phenomenology, would be to remove the Higgs boson from the spectrum entirely, and recalculate the decay widths of all sparticles. A consistent approach to this is handled in the pMSSM [18].

Based on this, we suggest that a compelling simplified model is $\widetilde{C}_1^{\pm}\widetilde{C}_1^{\mp}$ and $\widetilde{C}_1^{\pm}\widetilde{N}_2$ production, with $\widetilde{C}_1 \to W^{(*)}\widetilde{N}_1$ and $\widetilde{N}_2 \to Z^{(*)}\widetilde{N}_1$ or $\widetilde{N}_2 \to h\widetilde{N}_1$. The three-body decays to off-shell W or Z bosons come into play when the mass splitting between mother and daughter is small. $M_{\widetilde{C}_1} = M_{\widetilde{N}_2}$ is a motivated choice, but $M_{\widetilde{N}_1}$ should be considered arbitrary. In the cMSSM, there is model dependence arising from the $\widetilde{q}$ contributions in the matrix-element calculation of the production cross section. The $\widetilde{q}$ Feynman diagrams are much less significant (numerically) than the Standard Model gauge boson ones, which arise naturally from the neutralino/chargino kinetic energy piece in the Lagrangian. Reference cross sections can be chosen accordingly, ignoring $\widetilde{q}$ contributions. Because of the importance of gauge boson diagrams, $\widetilde{C}_1^{\pm}\widetilde{N}_2$ production is roughly twice as large as $\widetilde{C}_1^{\pm}\widetilde{C}_1^{\pm}$ production, and $\widetilde{C}_1^{+}\widetilde{N}_2$ production is roughly 60% larger than $\widetilde{C}_1^{-}\widetilde{N}_2$ production. This mirrors the behavior of W^* and γ^*/Z^* in the Standard Model.

Even though we have downplayed the pair production of heavy-flavor squarks, this view may be too model dependent. Contours of stop and sbottom mass for the cMSSM points considered here are shown in Fig. 19 of the Appendix. A very large splitting between the stop and/or sbottom and the other squark masses is not obtained (except for small m_0 and $m_{\frac{1}{2}}$) for these choices of cMSSM

parameters. The stop is special in the MSSM, whether based on fine-tuning arguments or its relation to the Higgs boson mass, and one mass eigenstate may be significantly lighter than most other sparticles. Later, we observe that the acceptance for tb events is high for generic hadronic selections. Targeted analyses, which may leverage the presence of b or t quarks in the final state, could have a much larger acceptance. Here, we will consider a scenario where $\widetilde{N}_1, \widetilde{t}$ and $\widetilde{g}$ are the only relevant sparticles in our current energy regime. Figure 9 shows the relation between gluino and stop pair production as a function of mass, where the gluino mass has been offset by the top mass (175 GeV) to emphasize the kinematic limit for $\widetilde{g} \to \widetilde{t}\bar{t}$. For a stop mass of 300(600) GeV, a gluino of mass 550(950) GeV has a comparable production cross section; for smaller mass splittings, gluino production will provide more stop events, with additional t quarks in the final state (half with the same sign).

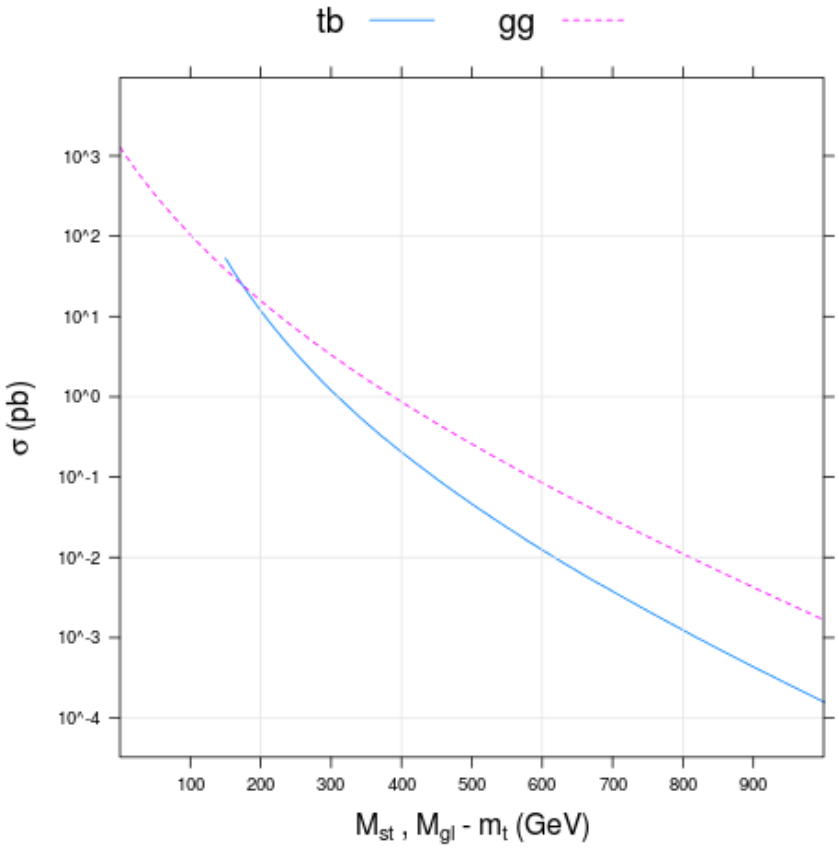

Figure 9. A comparison of stop-antistop and gluino pair production as a function of mother mass. The gluino mass $M_{\widetilde{g}}$ is offset by $m_t = 175$ GeV, the kinematic limit for the decay $\widetilde{g} \to \widetilde{t}\bar{t}$.

4 Studies of the *Jets+mHT* and α_T Analyses

In this section, we justify our previous statement that an analysis of the production cross section is meaningful. To this end, we have performed a generator-level analysis that replicates the *Jets+mHT*

and α_T event selections. These two analyses are the most straight-forward to reproduce (we leave m_{T2}, which requires a hemisphere decomposition of events and an iteration over invisible particle candidates, for a further study). Details of the experimental analyses are to be found in the earlier references. There are several results we wish to convey. The first two demonstrate that the current analyses are indeed sensitive to the dominant processes, though in different ways. A third shows the overlap between the two analyses. The last is to comment on the impact of a leptonic veto on these selections. A discussion of the role of extra radiation of quarks and gluons in the analysis results is presented in the next section.

Figure 10 shows the acceptance of events in the $(m_0, m_{\frac{1}{2}})$ plane, broken down by process type for the *Jets+mHT* analysis.[2] Only six of the process classes are significant. For this plot, the acceptance is defined as the number of events that pass the event selection per category, divided by the total number of events studies for that value of $(m_0, m_{\frac{1}{2}})$. The plot demonstrates that the *sg*, *ss*, and *nn*

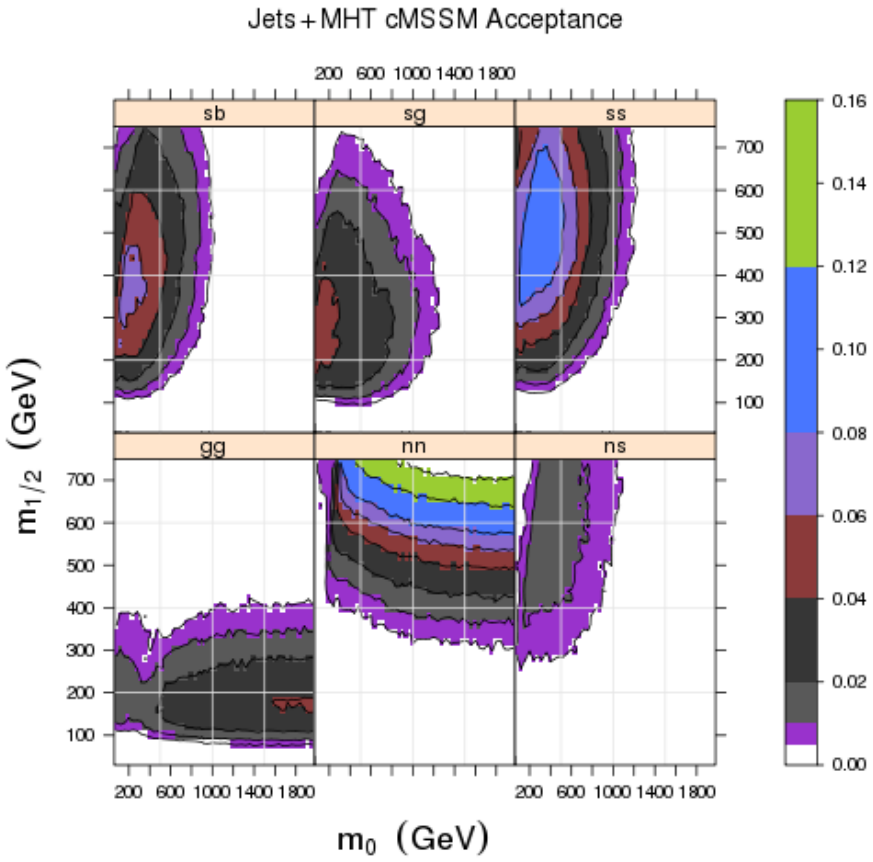

Figure 10. The acceptance (number of events that pass cuts divided by the total number of events generated at the model point) broken down by subprocess type for the *Jets+mHT* analysis.

process classes are the most significant after applying the selection cuts. The contours of acceptance reflect the contours of total cross section shown in Fig. 2. This implies an acceptance that is relatively

[2]We apply the Baseline cuts of $(H_T, \not{H}_T)$ >(350,200) GeV. See the Appendix for other details.

independent of process type, provided that the primary sparticle masses are similar. The *nn* process exhibits a turn-on associated with the $\not{E}_T$ threshold in the selection.

A related quantity is the efficiency of an individual process in isolation from the other processes in a full model, like the cMSSM. This efficiency is the relevant one needed for a simplified model analysis. Figure 11 shows this unbiased acceptance in the $(m_0, m_{\frac{1}{2}})$ plane by processes type for the *Jets+mHT* selection. This analysis has a high efficiency for most types of processes, except for the *nn* class, and *gg*

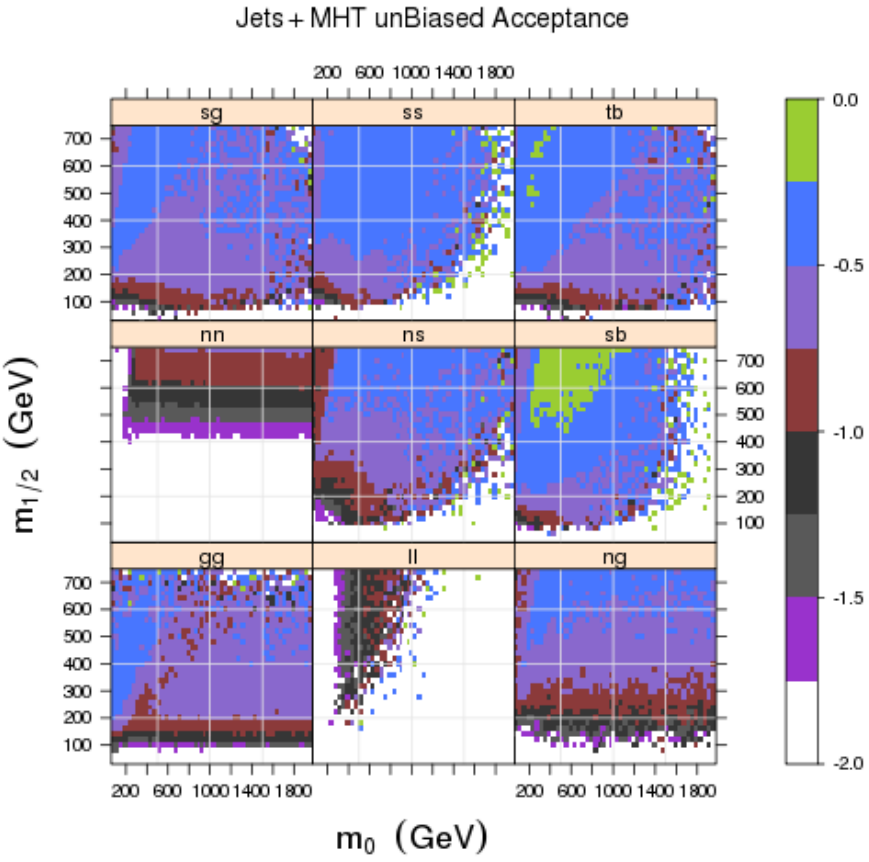

Figure 11. The acceptance (number of events that pass cuts divided by the total number of events generated at the model point for the given process) broken down by subprocess type for the *Jets+mHT* analysis. The contours are drawn in a $\log_{10}$ scale.

for lower $M_{\tilde{g}}$. There are still correlations built into these results; for example, the *ss* process depends upon the gluino mass. However, the effect on kinematics is less than that on production rates, as observed earlier.

The behavior of the *nn, gg, ng* acceptance is relatively easy to interpret. All the gaugino masses are roughly set by $m_{\frac{1}{2}}$ independent of m_0, and the mass scales sets the hardness of the kinematics, and, hence, the selection efficiency. Too low values of $M_{\widetilde{C}_1}, M_{\widetilde{N}_2}$ will yield too low $\not{E}_T$ to pass these selections. The *sg* acceptance is less obvious. There is some loss of efficiency near the diagonal line. From Fig. 18 in the Appendix, we observe that this coincides with $M_{\tilde{g}} \sim M_{\tilde{q}}$. We expect that squark

decays to a soft jet and the gluino, and the gluino efficiency is lower because of 3-body decays.

We have performed a similar analysis for the α_T event selection, displayed in Figs. 12 and 13. The

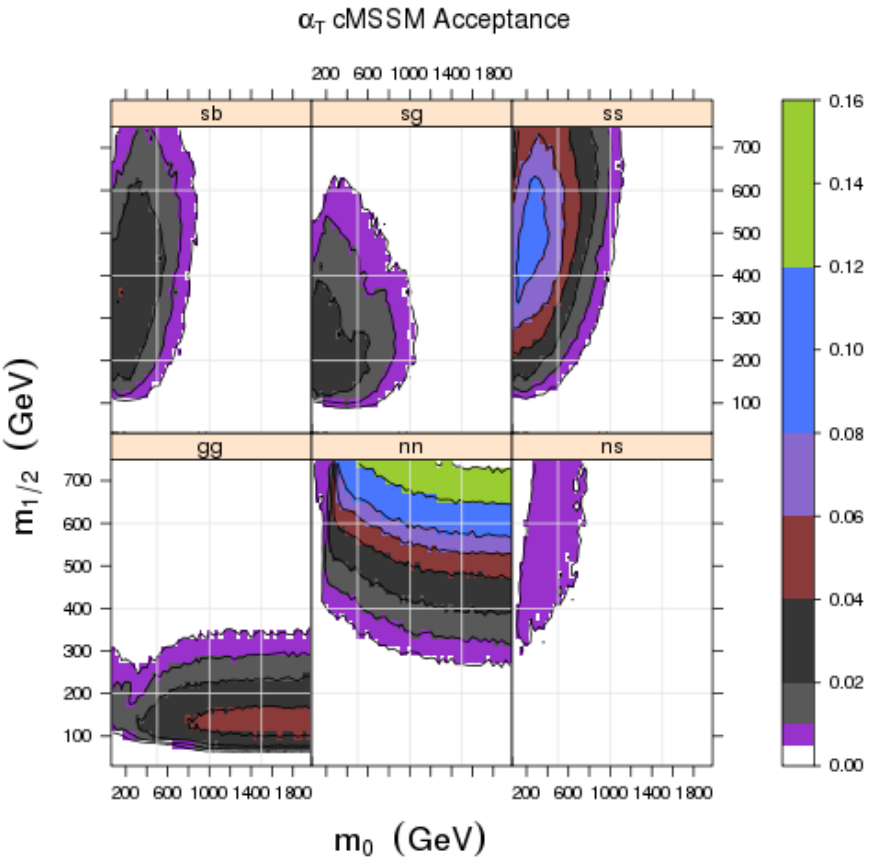

Figure 12. The acceptance (number of events that pass cuts divided by the total number of events generated at the model point for the given process) broken down by subprocess type for the α_T analysis.

acceptance in the cMSSM is similar, but different, from that in the *Jets+mHT* selection. The similarity is somewhat surprising, given that α_T focuses on the two leading jets, and their relative angle, which is characteristic of $\widetilde{q}\widetilde{q}^*$ production.[3] The acceptance per process is shown in Fig. 13. There are patterns which are similar to those in Fig. 11, particularly the loss of efficiency near $M_{\widetilde{g}} \sim M_{\widetilde{q}}$.

Given the similarity of the exclusion limits (Fig. 1) and the acceptance for the two selections, one wonders whether the two analyses are highly correlated, despite the different cuts. In Fig. 14, we address the overlap between the two selections, by calculating the acceptance of events that pass both selection requirements. Here, we show the fraction of events that pass both selections relative to those that pass the *Jets+mHT* selection. The overlap ranges from 20-50% depending on the process and point in the $(m_0, m_{\frac{1}{2}})$ plane. There is less overlap for $\widetilde{g}\widetilde{g}$ production and decay, and more for $\widetilde{q}\widetilde{q}$ topologies. This suggests that a combination of these selections would be beneficial.

[3] α_T handles the case of multiple jets by combining them into two pseudo-jets, whose kinematics are used in the naive two-jet formula. This recombination helps recover some jet energy lost to final state radiation.

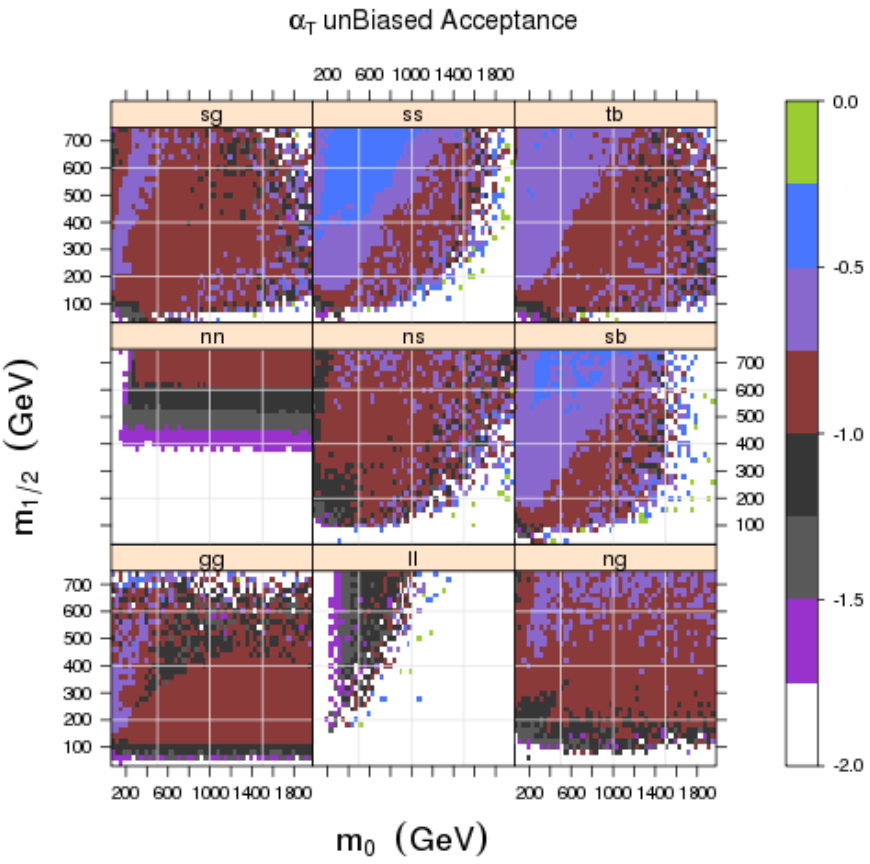

Figure 13. The acceptance (number of events that pass cuts divided by the total number of events generated at the model point for the given process) broken down by subprocess type for the α_T analysis. The contours are drawn in a $\log_{10}$ scale.

There is one last issue regarding the hadronic analyses that we wish to address: the impact of the lepton veto. A veto is applied on events that have an electron(muon) in the central rapidity region of the detector ($|\eta| < 2.5$) with $p_T > 10(15)$ GeV to reduce backgrounds. In Figure 15, we show the fraction of events that fail the *Jets+mHT* selection when the lepton veto is applied at the end. The impact of the veto can be severe. The increase near $m_0 = 900$ GeV and $m_{\frac{1}{2}} = 400$ GeV can be attributed to the turn-on of the decay $\widetilde{g} \to \widetilde{t} + \bar{t}$, where the $\widetilde{t}$ can also decay to a t. As we gain confidence in our modeling of Standard Model backgrounds, we may be able to apply more sophisticated cuts that reduce the backgrounds without sacrificing signal. This particular example also illustrates that simplified models that are too simple may not be able to catch all the complexities of a particular model.

5 Other Phenomenological Considerations

One may well wonder why $\widetilde{q}\widetilde{q}$ production and decay passes an event selection requiring 3 or more jets, or why $\widetilde{g}\widetilde{g}$ production is not constrained at the same level. The presence of additional jet activity can

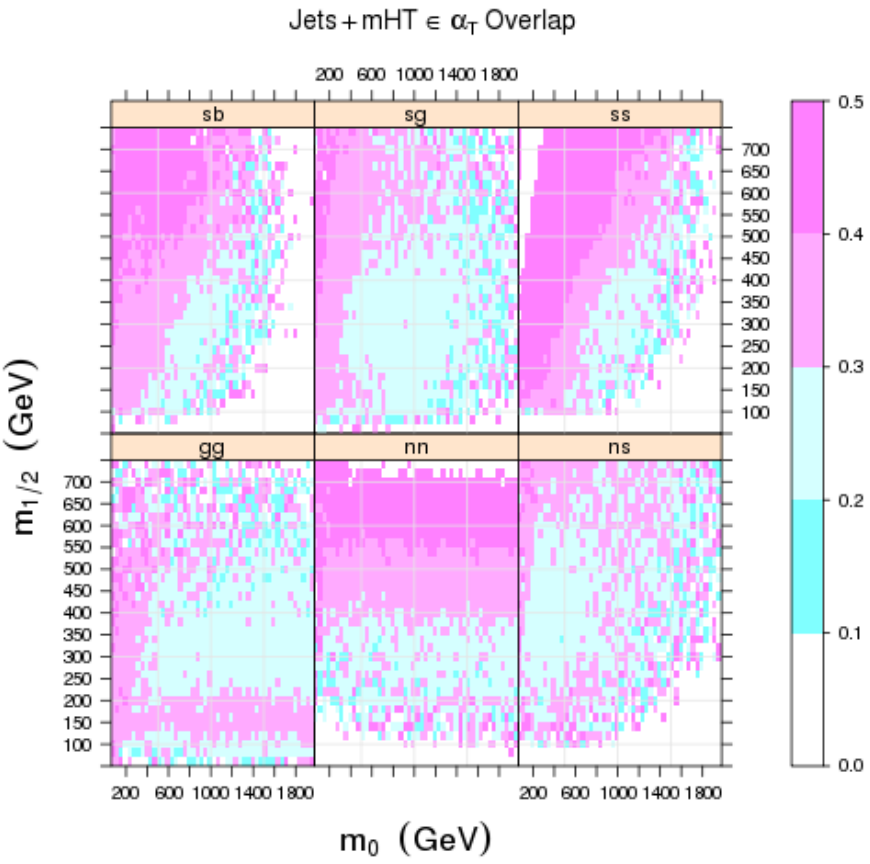

Figure 14. The fraction of events that pass both selections relative to the events that pass the *Jets+mHT*.

arise from the evolution of partonic structure through initial or final state radiation (ISR or FSR). The probability that a quark produced in the decay of a heavy squark at the scale $Q_F \sim M_{\tilde{q}}$ will remain a single parton down to the jet resolution scale is given by the Sudakov form factor, approximately:

$$\exp\big(-\frac{\alpha_s}{2\pi}C_F \ln^2\big(\frac{M_{\tilde{q}}^2}{p_T^2}\big)\big).$$

Choosing $M_{\tilde{q}} = 500$ GeV and $p_T = 50$ GeV, we estimate this probability at roughly 40%, or 16% when considering a pair of squarks. Clearly, vetoing a third jet would significantly reduce the signal acceptance. The modeling of FSR, while not free from theoretical ambiguity, has been studied in some detail at LEP (though for a color singlet system) and in top decays at the Tevatron. The estimate of ISR is less under control, because of the dependence on parton distribution functions and the choice of phase space for parton emission. Jets from ISR will tend to be uncorrelated with the produced sparticles, whereas a selection that includes jets from FSR might recover some of the resonant structure in the signal process.

Figure 16 shows the fraction of events at each $(m_0, m_{\frac{1}{2}})$ point that pass the *Jets+mHT* selection with an additional jet from ISR. The origin of a jet is traced using Monte Carlo truth information and the highest-p_T quark or gluon constituent of a jet. Typically 20-30% of the jets arise from ISR.

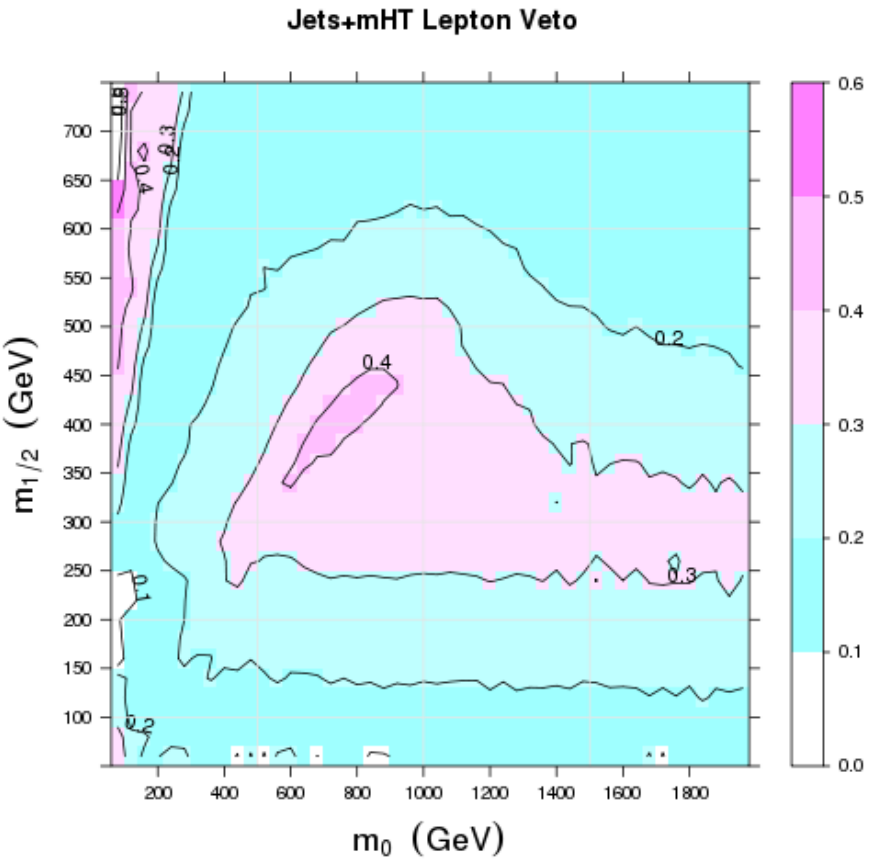

Figure 15. The fraction of events that fail the *Jets+mHT* selection because of a veto on identified leptons.

The region where the gluino is excluded relies more significantly on ISR, presumably because of the softening of the jet spectra and $\not\!\!E_T$ through the 3-body decay $\widetilde{g} \to q\bar{q}\widetilde{N}_1$.

The cMSSM has typically large intrinsic $\not\!\!E_T$, because of the large mass splitting between the $\widetilde{q}/\widetilde{g}$ and $\widetilde{N}_1$. Also, the existence of cascade decays leads to additional hard jets in the final state. This ameliorates some of the dependence on ISR. On the other hand, more general spectra, which lead to different mass splitting, will be more or less sensitive to ISR. Figure 17 shows the effect of the mass splitting for $\widetilde{q}\widetilde{q}$ events that pass the *Jets+mHT* event selection. Only the decay $\widetilde{q} \to q\widetilde{N}_1$ is allowed. The upper plot, with a fixed mass splitting of 100 GeV, shows a strong dependence on ISR. The lower plot, where $M_{\widetilde{N}_1}$ is fixed at 100 GeV, shows a more balanced dependence on ISR and FSR. Some regions of Fig. 16 which overlap with the parameters in the lower part of Fig. 17 have $\widetilde{q}$ cascade decays, such as $\widetilde{q} \to q\widetilde{N}_2(\to q\bar{q}\widetilde{N}_1)$, and thus less dependence on in ISR. Cascade decays, however, are more likely to produce at least one lepton in the final state, leading to a loss of acceptance with a leptonic veto.

The issue of the impact of ISR and FSR on high-p_T searches needs to be studied carefully. To date, some basic studies have been performed [22–24], but these do not address theoretical uncertainties. Currently, the systematic uncertainties assessed on the experimental limits, by increasing or decreasing

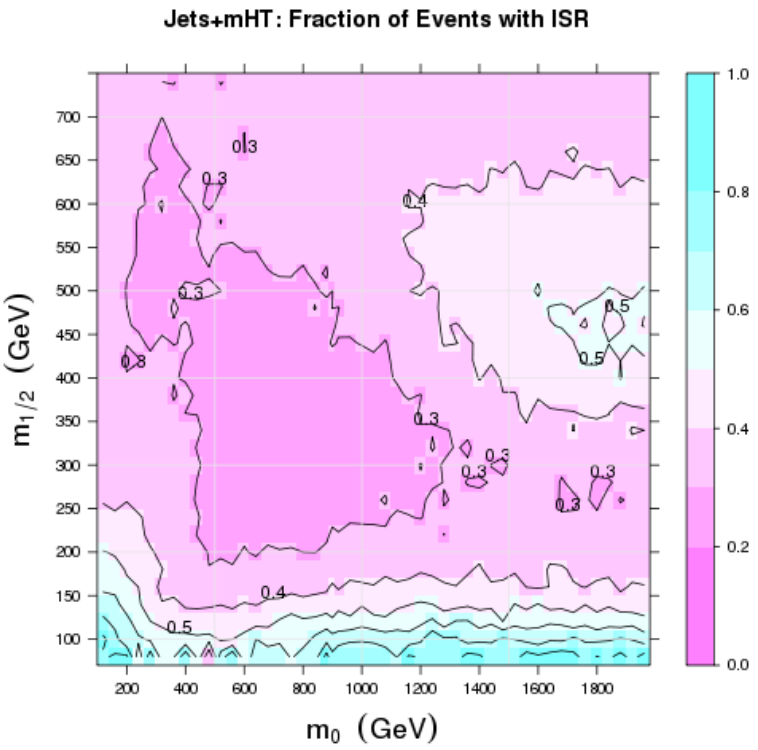

Figure 16. The fraction of events that pass the *Jets+mHT* selection with an additional jet from ISR in the cMSSM plane $(m_0, m_{\frac{1}{2}})$ for $\tan\beta = 10$.

the amount of radiation, are conservative. A better description could allow us to set more stringent limits on new particle production, or can be leveraged as a tool for discovery. Data driven techniques would be beneficial, perhaps based on observables from $t\bar{t}$ production (particularly $p_T(t+\bar{t})$).

6 Conclusions

The textbook signature for SUSY at hadron colliders is *Jets+*$\not\!\!E_T$, arising from the production and decay of the gluino $\widetilde{g}$ and the squarks $\widetilde{q}$. An analysis of the limits arising from hadronic SUSY searches by CMS, and interpreted in the cMSSM, shows the current limits are mainly excluding direct $\widetilde{qq}$ and $\widetilde{qg}$ production and decay. The exclusion of $\widetilde{qq}$ is an indirect exclusion of the the gluino $\widetilde{g}$ which mediates the process. Particle-level studies that follow the CMS event selections for the *Jets+mHT* and α_T analyses, show that the dominant processes at the cross selection level are also the dominant ones after cuts. Our study also quantified the overlap between the two different selections (20-50%, depending on the process) and the impact of the lepton veto (up to a 50% loss of events).

The importance of $\widetilde{qq}$ and $\widetilde{qg}$ is interesting, since interpretations of the data beyond the cMSSM often assume $\widetilde{qq}^*$ and $\widetilde{gg}$ production. We suggest these new topologies and ranges of parameters for them. These processes need also to be considered for a construction of a cMSSM point in terms of simplified models.

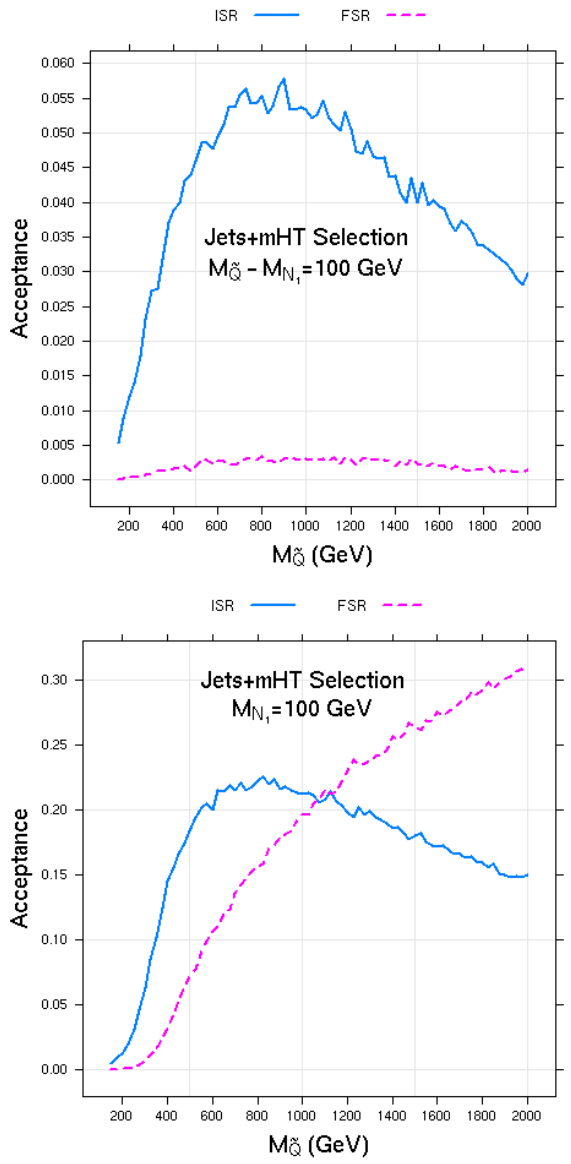

Figure 17. The acceptance of events passing the *Jets+mHT* event selection divided by their dependence on an ISR jet, for a fixed mass and varying mass splitting.

We also recognize the large potential of electroweak gaugino production for exclusion or discovery of SUSY. Beyond the current limits, chargino pair and neutralino-chargino production are the dominant processes. These processes also impact the leptonic searches for SUSY. In fact, the current CMS leptonic limits are bordering the region of the cMSSM plane (for the $\tan\beta = 10$ slice) where the second heaviest neutralino decays to a Higgs boson and the lightest neutralino.

Because of the relevance of $\widetilde{qq}$ production to the current limits, we studied in some detail the importance of initial state radiation for passing the SUSY search selections. For the cMSSM points

considered, final state radiation is more relevant, except for gluino masses less than $300 - 400$ GeV.

7 Appendix

Squark-Gluino Reference Plot

To ease the interpretation of figures displayed in the $(m_0, m_{\frac{1}{2}})$ plane, we collect here reference plots displaying contours of physical masses.

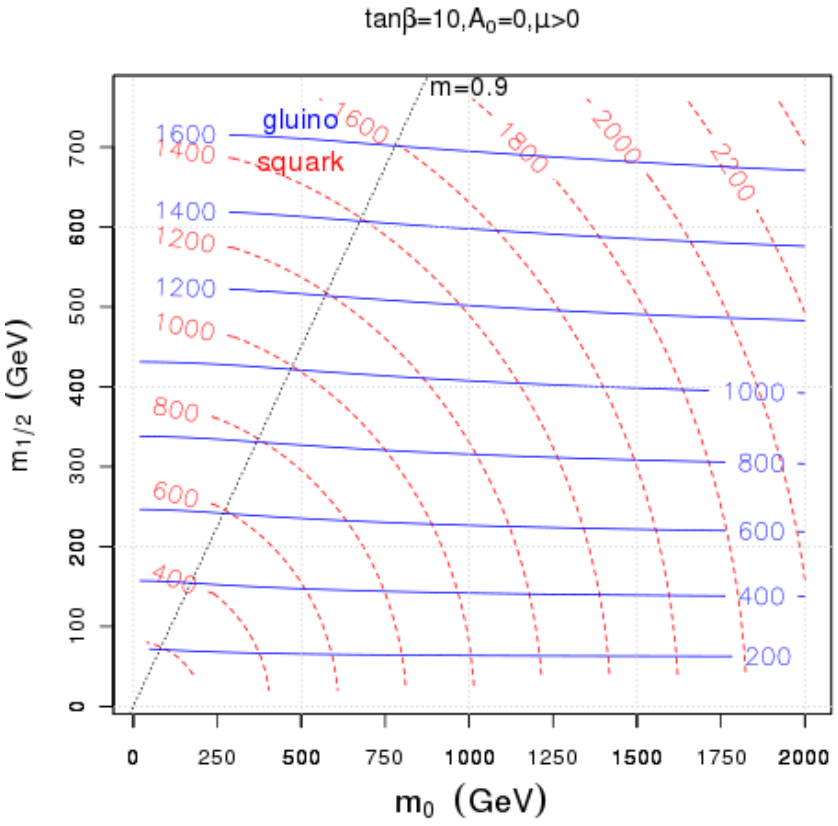

Figure 18. For reference, contours of squark and gluino masses in the cMSSM for $\tan\beta = 10, A_0 = 0$ GeV, $sgn(\mu) > 0$. A line with slope $m = 0.9$ has been superimposed to show the approximation correlation between $M_{\tilde{q}}$ and $M_{\tilde{g}}$.

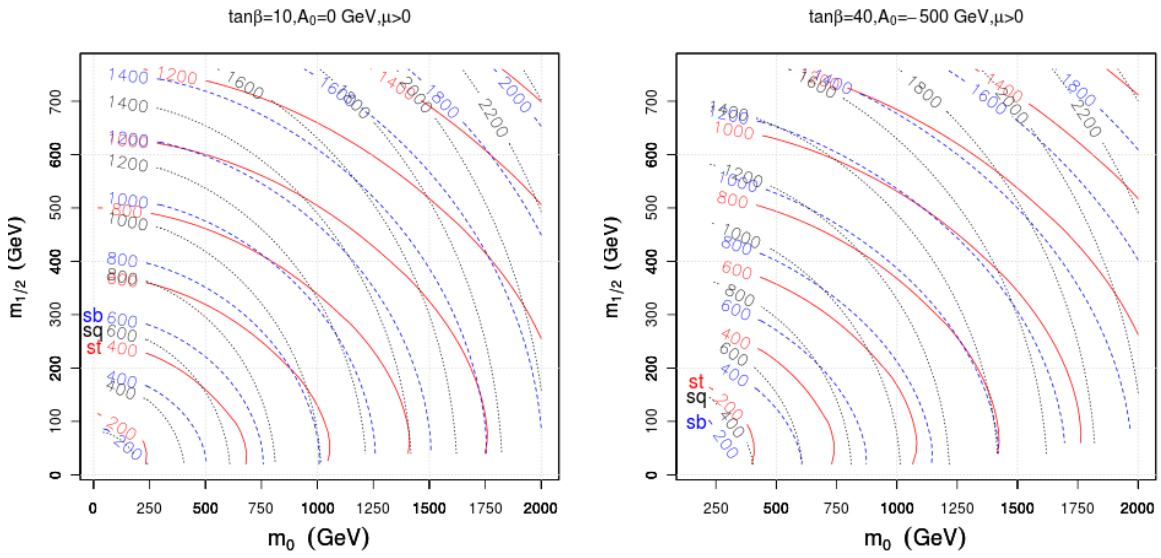

Figure 19. For reference, contours of sbottom, stop, and squark masses in the cMSSM for $\tan\beta = 10, A_0 = 0$ GeV, $sgn(\mu) > 0$ and $\tan\beta = 40, A_0 = -500$ GeV, $sgn(\mu) > 0$.

Dominant Processes for $\tan\beta = 40$

We present a similar plot as in Fig. 2, but for a cMSSM point with a large value of $\tan\beta$.

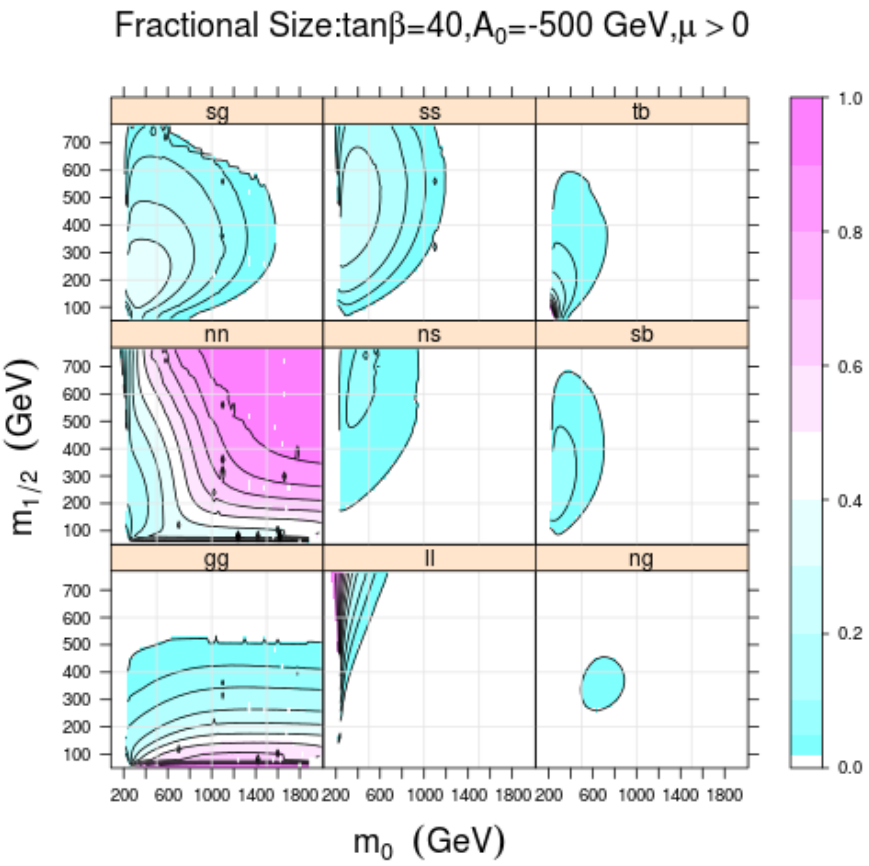

Figure 20. For reference, the fractional size of various subprocesses as a function of $(m_0, m_{\frac{1}{2}})$ for $\tan\beta = 40, A_0 = -500$ GeV, $sgn(\mu) > 0$.

Squark-Squark and Squark-Antisquark Differences

We provide additional information on the kinematic differences between $\widetilde{q}\widetilde{q}$ and $\widetilde{q}\widetilde{q}^*$ production, namely the distribution of the rapidity y of the $\widetilde{q}(\widetilde{q}^*)$.

Pseudo-Analysis Details

Here, we provide details on the tools used to simulate the detailed analyses performed by CMS, namely *Jets+mHT* and α_T. For each value of $(m_0, m_{\frac{1}{2}})$ considered, the `Pythia6`[25, 26] Monte Carlo was used to simulate the production, decay, and parton showering of sparticles. The p_T-ordered shower was used, with the underlying-event and hadronization effects turned off. Information about the progeny of jets was based on Monte Carlo truth information about the highest p_T parton inside the jet. Jets were defined using the package `FastJet` [27, 28].

The cuts applied are based on the description in the CMS analysis studies. The lepton veto is applied, again, using Monte Carlo truth information and leptons from hard decays.

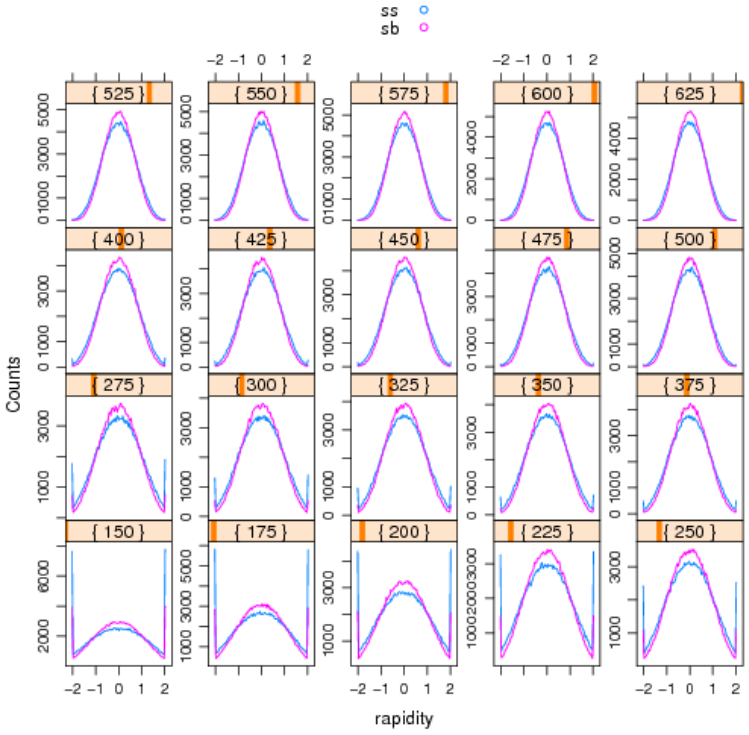

Figure 21. Comparison of the rapidity y of the produced $\widetilde{q}, \widetilde{q}^*$ for $\widetilde{q}\widetilde{q}$ versus $\widetilde{q}\widetilde{q}^*$ production.

Acknowledgments

The author thanks Seema Sharma for asking the correct questions about the *Jets+mHT* analysis in CMS that inspired this study, and to her, J. Lungu and J. Lykken for providing comments on the draft. S. Timm provided valuable help with running jobs on the Open Science Grid. This research was done using resources provided by the Open Science Grid, which is supported by the National Science Foundation and the U.S. Department of Energy's Office of Science. Fermilab is operated by the Fermi Research Alliance, LLC under Contract No. DE-AC02-07CH11359 with the United States Department of Energy.

References

[1] S. P. Martin, hep-ph/9709356.

[2] D. J. H. Chung *et al.*, Phys. Rept. **407**, 1 (2005), hep-ph/0312378.

[3] G. L. Kane, C. F. Kolda, L. Roszkowski, and J. D. Wells, Phys. Rev. **D49**, 6173 (1994), hep-ph/9312272;
H. Baer, M. Brhlik, Phys. Rev. **D53**, 597 (1996), hep-ph/9508321.

[4] https://twiki.cern.ch/twiki/bin/view/CMSPublic/PhysicsResultsSUS

[5] CMS Collaboration, CMS-PAS-SUS-11-004.

[6] CMS Collaboration, arXiv:1109.2352.

[7] CMS Collaboration, CMS-PAS-SUS-11-005.

[8] CMS Collaboration, CMS-PAS-SUS-11-015.

[9] CMS Collaboration, CMS-PAS-SUS-11-010.

[10] CMS Collaboration, CMS-PAS-SUS-11-011.

[11] W. Beenakker, R. Hopker, M. Spira, [hep-ph/9611232].

[12] B. Allanach, Comput. Phys. Commun. **143**, 305 (2002), hep-ph/0104145.

[13] A. Djouadi, M. Muhlleitner, and M. Spira, Acta Phys. Polon. **B38**, 635 (2007), hep-ph/0609292.

[14] P. Z. Skands *et al.*, JHEP **0407**, 036 (2004), hep-ph/0311123.

[15] B. Knuteson, S. Mrenna, [hep-ph/0602101].

[16] N. Arkani-Hamed, P. Schuster, N. Toro, J. Thaler, L. -T. Wang, B. Knuteson, S. Mrenna, [hep-ph/0703088 [HEP-PH]].

[17] D. Alves, N. Arkani-Hamed, S. Arora, Y. Bai, M. Baumgart, J. Berger, M. Buckley, B. Butler *et al.*, [arXiv:1105.2838 [hep-ph]].

[18] S. Sekmen, S. Kraml, J. Lykken, F. Moortgat, S. Padhi, L. Pape, M. Pierini, H. B. Prosper *et al.*, [arXiv:1109.5119 [hep-ph]].

[19] J. Alwall, P. Schuster, N. Toro, Phys. Rev. **D79**, 075020 (2009). [arXiv:0810.3921 [hep-ph]].

[20] V. Khachatryan *et al.* [CMS Collaboration], Phys. Lett. **B698**, 196-218 (2011). [arXiv:1101.1628 [hep-ex]].

[21] S. Chatrchyan *et al.* [CMS Collaboration], [arXiv:1106.4503 [hep-ex]].

[22] T. Plehn, D. Rainwater, P. Z. Skands, Phys. Lett. **B645**, 217-221 (2007). [hep-ph/0510144].

[23] R. Corke, T. Sjostrand, Eur. Phys. J. **C69**, 1-18 (2010). [arXiv:1003.2384 [hep-ph]].

[24] J. Alwall, M. -P. Le, M. Lisanti, J. G. Wacker, Phys. Rev. **D79**, 015005 (2009). [arXiv:0809.3264 [hep-ph]].

[25] T. Sjostrand, S. Mrenna, and P. Z. Skands, JHEP **0605**, 026 (2006), hep-ph/0603175.

[26] T. Sjostrand, S. Mrenna, and P. Z. Skands, http://projects.hepforge.org/pythia6/, version 6.4.25

[27] M. Cacciari, G. P. Salam, Phys. Lett. **B641**, 57-61 (2006). [hep-ph/0512210].

[28] M. Cacciari, G.P. Salam and G. Soyez, http://fastjet.fr/, version 2.3.4.